Formation of $\{11\bar{2}1\}$ twin boundaries in titanium by kinking mechanism through accumulative dislocation slip

Shenbao Jin, Knut Marthinsen, and Yanjun Li*

Department of Materials Science and Engineering, Norwegian University of Science and Technology, 7491 Trondheim, Norway

***Corresponding author: Y.J. Li (Yanjun.Li@ntnu.no)**

Abstract

The twinning behavior and kinking behavior of a commercial purity Ti subjected to room temperature dynamic plastic deformation (DPD) has been studied. Three types of deformation twins, $\{10\bar{1}2\}$, $\{11\bar{2}2\}$ and $\{11\bar{2}1\}$, have been observed. It is found that a considerable fraction of the $\{11\bar{2}1\}$ twin crystals were encompassed by the twin boundary segments in connection with kink band boundaries with much lower misorientation angles. A close investigation on the crystallographic nature of these deformation twins revealed that the $\{11\bar{2}1\}$ twin boundaries have evolved from deformation kink band boundaries through accumulative slip of single basal-$\langle a \rangle$ dislocations. This mechanism for the formation of twin boundaries is different from the known mechanisms through deformation twinning in metals, for which the twin orientation relationship has been achieved once the twin embryo is nucleated. The mechanism for the formation of kink band, the transformation from kink band boundary to deformation twin boundary and the further evolution of twin boundaries during DPD have been discussed in terms of Schmid factors of various dislocation slip systems.

1. Introduction

Twinning plays an important role in plastic deformation of hexagonal close-packed (HCP) metals due to insufficient dislocation slip systems. The most commonly observed twinning systems during conventional deformation, rolling and compression at room temperature in commercial purity (CP) Ti are $\{10\bar{1}2\}$ tensile twins (T1) and $\{11\bar{2}2\}$ contraction twins (C1) [1-4]. Though rarely, $\{11\bar{2}1\}$ twins (T2) can also be observed in as-rolled CP Ti [5,6]. At deformation temperatures higher than 400°C, $\{10\bar{1}1\}$ type compression twins (C2) becomes the predominant twinning mode [4,7]. It has been found that all four types of twins can be activated by the equal channel angular pressing at room temperature [8-11]; while the less common $\{11\bar{2}4\}$ twinning could form in high-purity Ti subjected to ballistic impact [12] or dynamic plastic deformation (DPD) at RT [13]. These results indicate that the deformation conditions (strain rate and temperature) have strong influence on the twinning modes. Though considerable work have been conducted on characterization of the twin structures developed during various deformation methods, the twinning mechanism in HCP metals is still not completely understood.

As known, a shuffle mechanism, in addition to pure glide of twinning dislocations, is usually necessary for most of the twinning modes in HCP metals [4,14]. However, among the above mentioned twinning modes, T2 is special since it is the only twinning in which all lattice sites are correctly sheared to their twin positions, and lattice shuffles are thus not required. Different nucleation mechanisms have been proposed for T2 twinning, for example, the zonal mechanism by dissociation of $\langle c \rangle$ slip dislocations [15], a combined reaction of $\langle a \rangle$ and

$\langle c+a \rangle$ slip dislocations to produce a 12-layer twin nucleus ($12 \cdot \frac{1}{36}\langle \bar{1}\bar{1}26 \rangle$) [16], or nucleation from a core structure of a $\frac{1}{3}\{11\bar{2}2\}\langle \bar{1}\bar{1}23 \rangle$ edge dislocation [17]. Besides, Capolungo and Beyerlein [18] proposed that the stable twin fault loops on $\{11\bar{2}1\}$ planes can form through double dissociation of a perfect basal or prismatic dislocation. In a molecular dynamics simulation of twinning in coarse grained Mg by Aghababaei and Joshi [19], T2 twin embryo was found to nucleate at the dissociation point via nucleation of twinning dislocations along the $\langle 11\bar{2}6 \rangle$ direction and with a Burgers vector of 0.1 nm, which is in the same range as calculated for the Burgers vector $\frac{1}{36}\langle 11\bar{2}6 \rangle$. On the other hand, through a TEM investigation of T2 twin structures formed in DPD-ed polycrystalline Co, Zhu et al. [20] suggested that dissociation of full basal dislocations plays an important role in the nucleation of T2 twins. Note that for all the proposed twinning mechanisms for known twins, a fast nucleation process is always involved [4,21], and the twin orientation relationship with respect to the grain matrix is achieved once the twin nucleated.

On the other hand, it has been extensively reported that T2 twins have a close crystallographic relationship to kink bands. According to Lane et al. [22], T2 twin is a special kink band in which basal-$\langle a \rangle$ dislocations are aligned in the boundary plane on every other basal atomic plane. In HCP graphite, the formation of T2 twins was supposed to be able to form solely by basal dislocation slip [23-25]. This formation model is in nature the same as that of kink bands proposed by Hess and Barrett [26]. Therefore, some researchers have argued that T2 twins in HCP metals can be regarded as a "geometry-fixed deformation kink band" [22,27] and thus are able to form solely by basal dislocation slip. However, this twinning mechanism has never been

validated by any experimental results.

In the present paper, based on a close investigation of T2 twins formed in a CP Ti subjected to DPD, we have revealed a mechanism for formation of T2 twin boundaries different from the previously proposed twinning mechanisms of all the known twinning modes , i.e. a gradual evolution from kink band boundaries to T2 twin boundaries through basal dislocation slips.

2. Experimental

CP Ti (ASTM grade 1) with a chemical composition (wt. %) of 0.03 C, 0.0009 H, 0.008 N, 0.12 O, 0.06 Fe and Ti (balance) was used for DPD experimental work. Here, DPD is a deformation method developed to realize high strain rate deformation of low stacking fault energy materials as well as HCP materials [13,28-32]. Cylindrical samples with dimensions of Ø16×24 mm were machined for the DPD process. Before deformation, electron backscattered diffraction (EBSD) analysis was conducted on the compression plane, in order to show the initial microstructure and the texture level with respect to the compression force. During DPD, the samples were deformed by multiple mono-directional impacting loading using an upper anvil in a drop tower at RT with a strain rate in the range of 10^2-10^3 s^{-1}. During each impact, the height reduction of the sample was 2 mm. The deformation strain was calculated by $\varepsilon=ln(L_0/L_f)$, where L_0 and L_f are the initial and final sample thickness, respectively. The maximum accumulative strain which Ti samples could tolerate (without cracking) during DPD is 1.13, corresponding to 8 DPD impacts. 6 samples subjected to different number of impacts, 1, 2, 3, 4, 6 and 8, corresponding to deformation strains of 0.09, 0.20, 0.29, 0.41, 0.71 and 1.13, respectively, were

obtained. The deformation structures of all the DPD samples were examined in the longitudinal sections by EBSD scanning. A calculation of Schmid factors of grains and kink bands was carried out based on the orientation of crystals determined by EBSD measurements. More detailed information about the DPD process and the accompanied EBSD analysis can be found in Ref. [33].

3. Results and discussion

3.1 Initial microstructure

Fig. 1(a) presents an EBSD image of the typical initial microstructure of a DPD sample in the compression plane. As indicated, the average grain size of the initial sample was ~20 μm. The initial texture is shown in Fig. 1(b) in terms of (0001) and $(10\bar{1}0)$ pole figures. These indicate that most of the c-axes lie in range of 60º-90º of the compression direction (CD). During compression, these grains were subjected mainly to c-axis extension, which promoted formation of $\{10\bar{1}2\}$ tensile twins. On the other hand, according to Akhtar et al. [34], $\{11\bar{2}1\}$ tensile twinning tends to be activated during compression when the angle between c-axis and CD is in range of 47º-60º.

3.2 Twins formed in samples deformed by DPD

It was found that the sample as deformed to an accumulated strain of ~0.29 (3 impacts) had the largest twin fraction. The decrease of the twin fraction at higher deformation strains is mainly attributed to the increase of critical shear stress for twining activation with grain refinement during deformation, which makes the twinning more difficult. At the same time, more grain boundaries will form due to dislocation slip. As a consequence, the twin boundary fraction

(the ratio between the length of twin boundaries to the total length of all types of grain boundaries) will decrease with increasing strain, although the absolute length of twin boundaries per volume could further increase. Fig. 2 presents the microstructure of the DPD sample with ε = 0.29. As shown , three types of twins were activated during DPD including T1, T2 and C1, the boundaries of which are highlighted by red, blue and green colors, respectively (Fig. 2a). Fig. 2(b) shows the histogram of misorientation angles for the grain boundaries. Three significant peaks can be seen at around 33º, 65º and 87º, which correspond with the 35.0º $\langle 10\bar{1}0 \rangle$ (T2), 64.6º $\langle 10\bar{1}0 \rangle$ (C1) and 85.0º $\langle 2\bar{1}\bar{1}0 \rangle$ (T1) type twin boundaries (TBs), respectively. However, from the misorientation axes of the grain boundaries around the three peaks (shown in the insets), it can be seen that only part of the boundaries with misorientation axes of $\langle 10\bar{1}0 \rangle$, $\langle 10\bar{1}0 \rangle$ and $\langle 2\bar{1}\bar{1}0 \rangle$, respectively, are belonging to the three types of TBs. It is interesting to see that the peak misorientation angles corresponding to T2 twins are smaller at small strains ε = 0.20 and 0.29 while larger at a higher strain of ε = 0.41 than the theoretical angle of T2 twins. This is in contrast to misorientation peaks corresponding to T1 twin, which are always larger than the theoretical values.

A further study of the T2 TBs automatically labelled by the TSL OIM EBSD software shows that they are mostly present as segments connected with boundaries with misorientation angles much less than 35º (Fig. 2c and d). Fig. 3(a) shows an example of such twin boundary segments surrounding an elongated twin like grain (labeled as DB1) in the matrix of a large grain (grain 1). The misorientation angles of DB1 crystal to the surrounding matrix of grain 1 were measured along the grain boundary, as shown in Fig. 3(b). It shows that the misorientation angles

vary in the range of 24~36º, and the misorientation angle of upper side boundary is about 5º lower than that of the lower side. This is different from the character of typical deformation twins, which usually have symmetric TBs. The segments of grain boundaries between DB1 and grain 1 with misorientations in range of 34º to 36º were automatically identified as T2 TBs by the EBSD software, as labeled with blue color. The twin orientation relationship can be further confirmed by pole figures shown in Fig. 3(c), i.e., the crystal rotation in DB1 with respect to the surrounding matrix is around one of the $\langle 10\bar{1}0\rangle$ axes, as marked by black dashed circle in the $\{10\bar{1}0\}$ pole figure. Furthermore, the crystal of DB1 and the surrounding matrix have a pair of coincident $\{11\bar{2}1\}$ planes, the common trace of which at the sample surface is indicated by a black arrowed line in Fig. 3(a). This $\{11\bar{2}1\}$ plane trace is parallel to the trace of the grain boundary between DB1 and matrix, further confirming that the blue segments are T2 twin boundaries.

As can be seen in Fig. 3(a) and (d), the boundary segments encircled by the blue dotted lines and with lower misorientation angles have about the same boundary plane $\{11\bar{2}1\}$ and the same crystal rotation axis $\langle 10\bar{1}0\rangle$ as the T2 TBs. Two possible mechanisms are considered for the formation of such special boundaries between DB1 and grain 1: 1) the boundary segments with much lower misorientation angles than 35º have formed due to the misorientation decline of T2 deformation twin boundaries; and 2) the TB segments have evolved gradually from the boundaries with lower misorientation angles based on a new twinning mechanism.

It is common that the deformation twin boundaries lose their perfect twin misorientation due to the different lattice rotation behaviors of twin crystal and matrix crystal caused by

dislocation slip during further deformation. However, such a degradation of TBs usually causes the misorientation angles to increase. This is exactly the case for T1 and C1 twin boundaries subjected to further deformation strains, which will be discussed in section 3.4.3. Since the samples were subjected to a mono directional impact loading during DPD, it is impossible to destroy the twin orientation relationship of $\{11\bar{2}1\}$ twin boundaries by reducing the misorientation angle (from 35º to 24º in Fig. 3) while keeping the same rotation axis as well as keeping the same $\{11\bar{2}1\}$ grain boundary planes unchanged. To achieve such an evolution of twin boundaries, the same dislocation slip processes as those that caused twinning but with the opposite shear directions would have to be activated. But in such conditions detwinning will happen, which requires shrinkage of the deformation twins by migration of twin boundaries without changing the twin boundary misorientation. In this case, the twin boundary misorientation will stay the same. This means that the first mechanism is impossible while the special T2 twin boundaries in Fig. 3 may have formed by the second mechanism. To understand how this new type of TBs forms, it is important to study how the twin shaped grains and the surrounding boundaries with relatively lower misorientation angles formed during DPD.

3.3 Deformation bands formed in the DPD samples

3.3.1 Kink bands

A careful examination of the samples subjected to DPD at lower strains, $\varepsilon = 0.09$ and 0.20, shows that a large number of twin shaped deformation bands (DBs) with misorientation axes of $\langle 10\bar{1}0 \rangle$ to the surrounding grain matrix and enclosed by boundaries of relatively low misorientation angles (6-32^{o}) have already formed. Fig. 4(a) shows a tiny DB with

misorientation angles from 6º to 16º to the surrounding matrix (grain 5) formed in the sample of ε = 0.09 (one impact), and Fig. 4(b) shows a twin-shaped DB with misorientations from 16º to 32º to the surrounding matrix (grain 6) in the sample subjected to two impacts of DPD (ε = 0.20). The DBs in the two grains both have $\langle 10\bar{1}0 \rangle$ rotation axes. This crystallographic characteristic of the DBs are the same as the deformation kink bands frequently observed in HCP metals like Zn, Ti and Mg subjected to compression deformation [22,26,27,35,36], caused by single basal-$\langle a \rangle$ dislocation slip and having rotation axes of $\langle 10\bar{1}0 \rangle$. So these DBs should be termed as kink bands.

Deformation kinking is an important deformation mode in addition to slip and twinning, especially in the metals and alloys with strong plastic anisotropy. The term kink was first used by Orowan in 1942 [37] to describe the deformation bands formed in the axially compressed Cd and Zn single crystals. It has been found later that the kink bands are mostly activated under the circumstances that the deformation strain cannot be effectively or efficiently accommodated by conventional deformation modes of slip and twinning, which is in nature the same as the reason for formation of deformation bands [38,39]. One extreme case for forming kink bands in HCP crystals was illustrated by Hess and Barrett [26], where a large stress is loaded parallel to the basal plane and thus the basal slip cannot operate to carry the strain because of the negligible resolved shear stress; and then a region of highly localized deformation developed by the avalanche initiation, operation, and arrangement of basal dislocations, resulting in the formation of the kink band. Since the kink bands are generally formed through the progressive rotation of the lattice, the kink bands can be considered as the deformation bands resulting from the ordinary

slip process. It is assumed that the kinking deformation in HCP materials is mainly caused by the accumulation of basal or prismatic dislocation pairs and their motion in the opposite direction. Some recent computer analysis and experimental work suggest that the local operation of pyramidal dislocation may also play a role in the formation of pair of basal dislocations, and lead to the development of deformation kink bands [40,41]. The lattice rotation axis of the kink bands and the orientation of the boundary plane depend on the kind of the relevant active slip systems and the ratio of their operations, that is, the kink band boundaries are constructed by the edge dislocations of the active slip systems; and the rotation axis of the crystal will be perpendicular to both the slip plane normal and the Burger's vector of the dislocation [26,35,36]. In the following paragraphs, the crystallographic nature of the kink bands formed in the DPD samples will be examined in detail.

3.3.2 Boundary plane of the kink bands formed in the DPD samples

In previous studies on kink bands, less attention has been paid to the boundary planes of kink band and, to our knowledge, the kink bands boundary planes have never been experimentally determined. It is interesting to note here that the kink band and grain matrix in grain 5 in Fig. 4(a) have one set of almost parallel $\{11\bar{2}1\}$ planes (green dashed circles in the $\{11\bar{2}1\}$ pole figure), the traces of which are close to the trace of kink band boundaries. Fig. 4(b) shows another kink band with $\langle 10\bar{1}0\rangle$ type rotation axis but higher misorientation angles, in the range of 16.6 to 30.6º, to the surrounding matrix. The upper part of the kink band boundary is rather straight while the lower part is irregular. From the $\{11\bar{2}1\}$ pole figure in Fig. 4(e), it can be seen that the nearly coincident $\{11\bar{2}1\}$ planes of the kink band and matrix crystal encircled

by blue dotted lines have a misorientation angle of about 8.2º. The traces of both of the two $\{11\bar{2}1\}$ planes are close to the trace of upper kink band boundary. However, a further analysis shows that the kink band boundary trace is more close to the $\{11\bar{2}1\}$ plane trace of matrix crystal. Nevertheless the grain boundaries between the kink bands and the surrounding matrix in both Fig. 4(a) and (b) have the same crystallographic nature as those grain boundary segments connecting to the T2 twin boundary segments in Fig. 3, where the DB1 crystal in Grain 1 was speculated to be a kink band originally.

Fig 4 (f) shows a schematic drawing of Ti crystal indicating that two $\{11\bar{2}1\}$ planes with the same $\langle 10\bar{1}0\rangle$ rotation axis have an angle of 35.0º. During deformation kinking, the rotation of the kink band crystal and matrix crystal in opposite direction will make the angle between the two planes becoming smaller and smaller, which is equal to the difference between 35.0º and the misorientation angle between the kink band and matrix crystal. This is consistent with the experimental results shown in Fig. 4(e). The average misorientation angle of ~8.2º between the two closest $\{11\bar{2}1\}$ planes of kink band and matrix crystal is approximately the difference between 35.0º and 27º (average grain boundary misorientation angle between the kink band crystal and the matrix crystal). Once the two $\{11\bar{2}1\}$ planes of the kink band crystal and matrix crystal are overlapping with each other, the misorientation angle between the two crystals will be 35.0º. If the kink band boundary is also parallel to the coincident crystallographic $\{11\bar{2}1\}$ planes, the kink band crystal and the matrix crystal will fulfil the $\{11\bar{2}1\}$ twin relationship. This is exactly the case for the TB segments shown in Fig. 3.

3.3.3 Dislocation slip within the kink bands formed in the DPD samples

To confirm whether the kink bands have formed by single basal dislocation slip, the possible active dislocation slip systems have been evaluated by calculating the Schmid factors (SFs) of the kink band crystal (labeled as DB) and the surrounding matrix crystal (labeled as grain). Although the calculated SF values could not predict the dislocation slip of the original crystals, they can reveal part of the dislocation slip history because the gradual nature of lattice rotation of crystals caused by dislocation slip. In Ti, the basal-$\langle a \rangle$ slip and prismatic-$\langle a \rangle$ slip are much easier to activate than the pyramidal $\langle a + c \rangle$ slip, because the critical resolved shear stress (CRSS) for the former is much lower. According to Ref. [42-44], the CRSS of basal-$\langle a \rangle$ slip is only slightly higher than that of the prismatic-$\langle a \rangle$ slip. So in this study, only SF values of basal- and prismatic-$\langle a \rangle$ dislocation slip systems are calculated; and the slip systems with SF > 0.3 are arbitrarily considered to possess a high possibility to be activated. In a single crystal, if all the slip systems have SF < 0.3 (hard orientation), the slip system with the largest SF can still be activated to carry the deformation in spite of the low SF. However, in a polycrystalline material, the deformation of these grains with hard orientations will be accommodated by the surrounding grains with soft orientations, especially at relatively lower strains. Therefore, the threshold SF value for slip system activation was set as SF > 0.3 in this work.

For each kink band and the surrounding matrix crystal, 6 locations are selected along the kink band boundaries to calculate the corresponding SF values. The results are summarized in Fig. 5(a) and (b). Table 1 shows the example SF values of one location in the kink band crystal side and another in the matrix crystal side in each of the grains 1-6. As indicated, the SFs of all the prismatic slip systems both in the matrix of grain 1 and DB1 are less than 0.3. On the other

hand, the basal slip variants $(0001)[\bar{1}2\bar{1}0]$ of grain 1 and $(0001)[\bar{1}\bar{1}20]$ of DB1 have higher SF values than the other dislocation slip systems, i.e. 0.38 and 0.46, respectively. It suggests that prismatic-$\langle a \rangle$ slip is suppressed in grain 1 while the deformation of grain 1 is mainly carried by basal slip. As mentioned previously, the rotation axis of the crystal within kink bands will be perpendicular to both the slip plane normal and the Burger's vector of the dislocation. For the kink band caused by $(0001)[\bar{1}2\bar{1}0]$ or $(0001)[\bar{1}\bar{1}20]$ slip, the rotation axis will be $[10\bar{1}0]$ and $[1\bar{1}00]$, respectively. This is well consistent with the crystal rotation axes (Fig. 3c) measured directly from EBSD maps, confirming that the kink band DB1 in Grain 1 has formed by kinking due to the single $(0001)[\bar{1}2\bar{1}0]$ dislocation slip in grain matrix and single $(0001)[\bar{1}\bar{1}20]$ slip in kink band, which have the maximum SF values.

From the SF values of different slip systems of kink band crystals in grains 1-6 (Fig. 5 and Table 1), it can be seen that the prismatic-$\langle a \rangle$ slip systems all have low SF values (< 0.3) and thus greatly suppressed; while, in contrast, the SF values of the basal-$\langle a \rangle$ slip systems are not always higher than those of the prismatic-$\langle a \rangle$ slip systems in the surrounding matrix crystals. This is because the kink band crystal and surrounding grain matrix crystal could have different rotation extent during kinking. The high SF values of prismatic-$\langle a \rangle$ slip systems means that prismatic slip systems can also be activated in the matrix of these grains when subjected to further impact loading. Thus the rotation axis will deviate from the $\langle 10\bar{1}0 \rangle$ axes and the deformation by the same kinking mechanism can not continue.

Fig. 4(c) shows a kernel orientation spread map of grain 6. It can be clearly seen that the zones within the DBs as well as in the grain matrix close to the DBs both have high

misorientation gradients, which means that the DBs and the surrounding matrix have carried the deformation simultaneously. Though in many reports, the deformation bands or kink bands are suggested to be formed to accommodate most of the deformation strain of the grain, the slip behavior and thus the lattice rotation within the grain matrix are not necessarily frozen. According to Rosi's work [35], the lattice reorientation within the kink band even lags behind that of the surrounding matrix crystal after its formation. Considering that the lattices in kink band and grain matrix have rotated in opposite directions, the initial grain orientation should be in between of their orientations. Based on the SF values of different slip systems, it can be concluded that the twin-shaped DBs were formed in the grains with suppressed prismatic-$\langle a \rangle$ slip and having one active basal-$\langle a \rangle$ slip with a significantly higher SF value than the others. Since these DBs formed mainly through the kinking mechanism by single basal slip, their boundary walls are constituted of numerous basal dislocations [22,27].

Fig. 5(c) summarizes the impact loading direction according to the crystal orientations in 6 grains containing kink bands. As can be seen, all the loading directions are located in between the (0001) pole and $\{11\bar{2}0\}$ pole and close to the large circle of $\{10\bar{1}0\}$ plane. Such an orientation relationship between the loading direction and the grains will result in a low SF value for the prismatic-$\langle a \rangle$ dislocation slip and a rather high SF value for one single basal dislocation slip system, which favors the deformation kinking during impact loading of DPD.

When deformation proceeds, orientation of grains will change through crystal rotation. Then, the SF values for the single basal slip may decrease while those for other basal slip systems and prismatic slip systems would increase. If the latter exceeds the former in SF value, new slip

systems may operate, which will result into a deviation of the crystal rotation axis from $\langle 10\bar{1}0\rangle$. In that case, the T2 TBs may not form or the formed T2 twins through kinking will lose the twin orientation.

3.4 Evolution from kink band to twin

3.4.1 Crystal rotation around $\langle 10\bar{1}0\rangle$ caused by single basal-$\langle a\rangle$ slip

It is possible to examine in which conditions a T2 twin can form through a continuous single basal dislocation slip in a grain, assuming the grain has the same stress tensor as the macroscopic stress tensor of sample. The SF values of basal- and prismatic-$\langle$a$\rangle$ slip systems as well as T2 twin variants can be calculated as a function of rotation angle of the crystals from loading directions. To simplify the calculation, a rotation of loading direction by the angle θ from the crystal rotation axis $[10\bar{1}0]$ was selected. The basal-$\langle a\rangle$ slip variant of $(0001)[\bar{1}2\bar{1}0]$ (B2) was selected as the single dislocation slip system. The schematic drawing of the loading direction in relation to the crystal lattice is shown in Fig. 6. More detailed procedure on SF calculations in HCP materials can be found in Refs. [45] and [46]. The angle (θ) between the loading direction and $[10\bar{1}0]$, and the angle (ω) between the $[0001]$ direction and the projection line of loading direction in $(10\bar{1}0)$ plane are the parameters to determine the activity of different slip systems. In order to have B2 as the single slip system, some criteria have to be fulfilled. Here, we have arbitrarily set the criteria as: SF value of B2 is larger than 0.3 and is the largest among all basal-$\langle$a$\rangle$ slip systems while the SF values of all prismatic-$\langle$a$\rangle$ slip systems are less than 0.3. As can be seen, when $\theta < 50.8^{o}$, the SF values of slip system B2 are always smaller than 0.3, meaning that this slip system is difficult to activate (Fig. 6b); while when $50.8^{o} < \theta < 63.4^{o}$, the

basal slip system B3 $(0001)[\bar{1}\bar{1}20]$ and the prismatic slip system P1 $(\bar{1}100)[\bar{1}\bar{1}20]$, instead of slip system B2, are more likely to activate because of the higher SF values, though the SF value of B2 is larger than 0.3 in certain ω ranges, which will result in different rotation axes instead of $[10\bar{1}0]$. In contrast, when θ exceeds 63.4º, the basal slip systems B2 and B3 as well as the prismatic slip system P1 tend to be activated at different ω angles. For example, when θ = 70º (Fig. 6d), the SF value of B2 is larger than that of B3 in the ω angle range of 39º-50.5º while the SF values of prismatic-$\langle a \rangle$ slip variants are less than 0.3, thus a single dislocation slip of B2 is possible. However, considering that the SF value of B3 is also larger than 0.3 in this ω ranges and the difference of SF values of B2 and B3 is so small, it is possible that the B2 and B3 slip can be activated simultaneously. If these two slip systems operate equivalently, the rotation axis will be $[11\bar{2}0]$. In that case, no kink bands with $\{11\bar{2}1\}$ boundary planes will form. So it is difficult to form kink bands with $\{11\bar{2}1\}$ as boundary planes even when the θ angle is 70º (Fig. 6d).

As shown in Fig. 6(f), when θ > 85.2º, the SF value of slip system B3 becomes smaller than 0.3 and a single slip of B2 can be achieved within a relatively large ω angle range. The ω angle ranges for activation of a single $(0001)\langle\bar{1}2\bar{1}0\rangle$ slip at different θ are indicated by light green zones in Fig. 6(c)-(f), showing that the possibility for deformation by a single dislocation slip B2 increases with increasing θ angle. This is in agreement with Fig. 5(c), where the loading directions in grains 1-6 all have a very small angle to one of the prismatic plane. The maximum ω angle range for one single basal-$\langle a \rangle$ slip B2 to keep active, is 18.5º to 56.5º (Fig. 6f). Therefore, the maximum crystal rotation around $[10\bar{1}0]$ that favors single slip of

$(0001)[\bar{1}2\bar{1}0]$ is ~38º (Fig. 6f).

Considering the opposite rotation direction of kink band and matrix grain, the rotation angle is sufficient to reach the misorientation angle of T2 twin (35º) by rotating around $[10\bar{1}0]$ axis. This result confirms the possibility of formation of T2 twin boundaries through gradual kinking caused by accumulative single basal slip. For those twin boundaries formed by kinking, a further rotation beyond the twin misorientation by kinking based on the same single dislocation slip, or by different dislocation slip systems will cause the twin boundaries rotate away from the twin orientation relationship. For conventional deformation methods, in order to form similar T2 TBs through the kinking mechanism, the loading direction has to keep ideal angles to the basal plane and the $\langle 10\bar{1}0\rangle$ direction in terms of θ and ω, the chance of which is very low. Moreover, the SFs are calculated in the present paper based on the assumption that the stress state of each grain coincided with the macroscopic applied stress. However, considering that certain deviations could exist between the state of the macroscopically applied stress and the actual stress state for a particular grain, the slip systems with relatively lower SFs could also be activated. If more slip systems operate in the kink bands and grain matrix, the rotation axis will depart from $\langle 10\bar{1}0\rangle$, which further decreases the probability of forming T2 twin boundaries through this gradual slip process. These factors may account for why this kind of twin boundaries have never been reported before. However, due to the high strain rate and mono-directional loading natures of DPD process, once a single basal-$\langle a\rangle$ dislocation slip is activated, it may continue until the impact loading is finished, although the SF of other dislocation slip systems may change to higher values than the initial dislocation slip in the loading process. Such a hypothesis on the

"avalanche effect" of shock loading is supported by the experimental evidence that some of the T2 twin boundary segments (Fig. 3 and Fig. 8) formed by the kinking process have higher misorientation angles than 35°. In principle, the ideal twin misorientation will give a minimum twin boundary energy. However, impact loading with surplus energy could even deform the twin boundaries to an energetically less favorable state. This avalanche effect increases the possibility for the formation of $\{11\bar{2}1\}$ twins by kinking.

3.4.2 Formation of T2 twin boundaries through crystal rotation of kink bands

By examining the SF values of T2 twin variants in those grains with kink bands (Fig. 6b-f), it is found that at least one of the 6 variants of T2 twin can have a quite high positive SF value, implying that some of the T2 twin variants have a high potential to be activated in a conventional way. However, no conventional type T2 twins were observed in grains containing kink bands. This may be ascribed to the difference in CRSS between T2 and basal dislocation slip, i.e., the latter has a much lower CRSS value. Also, the shear strain provided by each single impact loading during DPD is rather small, which is not enough to activate T2 twins (theoretical shear strain 0.638) through conventional twinning mechanisms. This is different from the room temperature ECAP process of CP Ti, where a large fraction of conventional $\{11\bar{2}1\}$ twin crystals could form due to the high shear strain in each pass [11].

However, due to the complexity of the deformation of a multigrain structure, the shear strain achieved in some of the grains can be larger than the theoretical shear strain endured by a single crystal, therefore conventional $\{11\bar{2}1\}$ could also form. For example, the T2 twin in Fig. 2(e) could have formed through a conventional twinning mode, where the TBs along the two sides of

the twin crystal are continuous and symmetric.

It should also be mentioned that some kink bands could not develop into T2 twins during further impact loading if their orientation are unfavorable to keep the same single basal dislocation slip. In this case, new basal dislocation slip systems or prismatic dislocation slip systems may be activated, by which the rotation axes and the boundary planes of kink bands will deviate from $\langle 10\bar{1}0\rangle$ and $\{11\bar{2}1\}$, respectively. As an evidence, even different locations in the boundary of DB1 in Fig. 3(d) have different rotation axes than $\langle 10\bar{1}0\rangle$. Because of the complex stress configurations in the zones near grain boundaries, more slip systems such as second basal or prismatic slip in addition to the initially high SF single basal slip could be activated, resulting in a deviation of the rotation axis from $\langle 10\bar{1}0\rangle$, as indicated by black circles in Fig. 3(a) and (d). In that case, the segments of kink band boundaries close to grain boundaries cannot evolve into TBs. In contrast, single slip of basal dislocations in the middle part of kink bands maintains the rotation axis better because of relatively simple stress configuration (blue circles in Fig. 3a and d). This may be the reason why T2 TBs generally develop in middle part of kink bands.

Bullough [47] has proposed a growth mechanism of T2 twins, i.e. growth through localized $\langle 11\bar{2}0\rangle$ slip on K2 (0001) plane. This was recently discussed again by Wang et al. [6] because large orientation variation and irregular TBs were observed in some T2 twins in Ti. Even with these previous works, the twinning mechanism through continuous slip of DBs (or kink bands) has not been well considered. Here our work shows a first experimental evidence for the mechanism. Recently, a formation mechanism of incoherent twin boundaries in an Al-Mg alloy subjected to DPD through gradual evolution from copious low-angle DBs by lattice rotation was

suggested [48]. This formation mechanism of the incoherent twins is in nature similar to the present formation of twin boundaries by kinking mechanism.

Fig. 6 shows a schematic drawing for the evolution from kink band to twins. The formation of T2 twins through kink band in HCP titanium should be attributed to the limited dislocation slip systems. In some grains with certain orientations, only one slip system can be activated. For example, in the grain shown in Fig. 6(a) and (d) with θ=90º and ω=37.5º, only one basal slip, B2, is supposed to activate because of the far higher SF value of B2 than others. The lack of active slip systems in this grain facilitates the formation of a kink band structure during high strain rate deformation. In contrast to the deformation boundaries caused by complex cross slip, the DB boundaries caused by single slip system are relatively simple and regular. As shown in Fig. 6(b), (c) and (e), each side of the DB boundaries is constructed by the same type of edge basal dislocations, which is in nature similar to that of T2 twin boundaries. On the other hand, the operation of the single B2 slip in the DB and grain matrix induces the lattice rotation around the same axis of $[10\bar{1}0]$, but in opposite directions.

To determine the evolution path of the boundary plane for kink bands during deformation is more challenging. The habit plane of the symmetric kink caused by single basal slip was supposed to be $\{11\bar{2}0\}$ at small misorientations angles according to [26,36,47]. However, from the EBSD grain boundary trace analysis in the present work it seems that the habit plane is quite close to $\{11\bar{2}1\}$ plane of one of the cyrstals (band and matrix) and keeps the same during further rotation. A further detailed study on the evolution of kink band boundary plane with increasing misorientation angle is still needed.

3.4.3 Evolution of twin boundaries upon further deformation

Fig. 8 shows the fraction change of T2 twins with increasing deformation strain during DPD. The maximum length fraction of T2 twins was achieved at $\varepsilon = 0.29$. However, since more boundaries will be created during deformation because of grain refinement, the relative length fraction of T2 twins may decrease though their absolute length does not. According to the curve of T2 twin length in per unit area in Fig. 8, the absolute fraction of T2 twins increases until $\varepsilon = 0.41$, which means that more lower angle kink band boundaries have transformed into T2 TB segments during further impact loading.

In contrast to the T2 TBs connected to kink band boundaries with lower misorientation angles at low strains, T2 TBs were more frequently connected to boundary segments of misorientation angles higher than 35^{o} in the samples subjected to higher deformation strains, i.e. $\varepsilon = 0.71$ and 1.13, as shown in Fig. 9(a) and (b). These boundary segments are not identified as TBs by OIM analysis software due to the large deviation from the perfect twin orientation relation. As shown in Fig. 9(c) and (d), the rotation axes of these segments deviate from the theoretical misorientation axis of T2 twin, $\langle 10\bar{1}0 \rangle$. The decrease of the absolute length of T2 twin boundaries at $\varepsilon > 0.41$ (Fig. 8) should be attributed to the loss of twin orientation relationship of some of the T2 twins during further straining.

Similar misorientation change of twin boundaries is also observed for T1 and C1 twins. As can be seen from Fig. 10, grain boundary segments, which are not identified as twin boundaries by OIM analysis software, are connected to the T1 (Fig. 10a) and C1 (Fig. 10b) twin boundaries. All these boundary segments have higher misorientation angles than their corresponding

theoretical values. Besides, as shown in Fig. 10(c) and (d), the rotation axes of these non-TB segments clearly deviate from the theoretical misorientation axes of T1 and C1 twins, i.e. $\langle 11\bar{2}0\rangle$ and $\langle 10\bar{1}0\rangle$, respectively. Interestingly, no degraded twin boundaries with misorientation angles lower than theoretical values have been found. This should be due to the mono directional loading nature of DPD process. The lattice rotation of the twin crystals caused by dislocation slip during further deformation will mostly result in misorientation angle increase instead of reduction. The increase of misorientation angles of twin boundaries during further deformation has also been reported before [11,49]. Because the boundary segments connecting with TB segments shown in Figs. 2-4 have smaller misorientation than twins, we can further confirm that these boundaries have form by a kinking process rather than misorientation change process of twin boundaries.

4. Conclusion

In summary, the deformation twins formed in a CP Ti subjected to DPD have been experimentally studied. Three types of deformation twins, T1, T2 and C1 have been observed. Some of the $\{11\bar{2}1\}$ (T2) TBs differ from conventional T2 twins, where a large fraction of T2 TBs have formed through a gradual increase of misorientation angle of a kink band boundary caused by accumulative slip of single basal-$\langle a\rangle$ dislocations. The formation of such twin boundaries by kinking mechanism mainly occurs in the grains with one of the $\langle 10\bar{1}0\rangle$ axes perpendicular to compression direction, where the prismatic-$\langle a\rangle$ dislocation slip is suppressed while only one basal-$\langle a\rangle$ slip system is favorable. A Schmid factor calculation of different dislocation slip systems shows that such a mechanism for formation of T2 twin boundaries is

feasible. With further straining, due to the grain rotation, new type of dislocation slip systems will be activated and therefore both the kink band boundary planes and grain rotation axes will be offset from $\{11\bar{2}1\}$ planes and $\langle 10\bar{1}0\rangle$ axes, respectively. As a result, the twin boundaries will lose their twin misorientation. It is supposed that the special deformation mode of DPD in terms of high strain rate and mono-directional impact loading plays an important role in formation of the special T2 twin boundaries by kinking mechanism.

Acknowledgements

Financial support from Research Council of Norway, under the FRINATEK project 'BENTMAT' (Project number 222173) is gratefully acknowledged. We would like also to thank Prof. O. S. Hopperstad at NTNU, for the valuable discussion and the help with using the drop tower facility in the SIMLab.

References

[1] M.H. Yoo, J.K. Lee, Deformation twinning in h.c.p. metals and alloys, Phil. Mag. A 63 (1991) 987–1000.

[2] L. Wang, Y. Yang, P. Eisenlhr, T.R. Bieler, M.A. Crimp, D.E. Mason, Twin Nucleation by Slip Transfer across Grain Boundaries in Commercial Purity Titanium, Metall. Mater. Trans. 41A (2010) 421–430.

[3] W. Tirry, M. Nixon, O. Cazacu, F. Coghe, L. Rabet, The importance of secondary and ternary twinning in compressed Ti, Scr. Mater. 64 (2011) 840–843.

[4] J.W. Christian, S. Mahajan, Deformation twinning, Prog. Mater. Sci. 39 (1995) 1–157.

[5] N. Bozzolo, L. Lisa, A.D. Rollett. Misorientations induced by deformation twinning in

titanium, J Appl. Cryst. 43 (2010) 596–602.

[6] L.Y. Wang, R. Barabash, T. Bieler, W.J. Liu, P. Eisenlohr, Study of $\{11\bar{2}1\}$ Twinning in α-Ti by EBSD and Laue Microdiffraction, Metall. Mater. Trans. A 44 (2013) 3664–3674.

[7] N.E. Paton, W.A. Backoffen, Plastic deformation of titanium at elevated temperatures, Metall. Trans. 1 (1970) 2839–2847.

[8] D.H. Shin, I. Kim, J. Kum, Y.S. Kim, S.L. Semiatin, Microstructure development during equal-channel angular pressing of titanium, Acta Mater. 51 (2003) 983–996.

[9] Y.J. Li, Y.J. Chen, J.C. Walmsley, R.H. Mathinsen, S. Dumoulin, H.J. Roven, Faceted interfacial structure of $\{10\bar{1}1\}$ twins in Ti formed during equal channel angular pressing, Scr. Mater. 62 (2010) 443–446.

[10] Y.J. Chen, Y.J. Li, J.C. Walmsley, S. Dumoulin, P.C. Skaret, H.J. Roven, Microstructure evolution of commercial pure titanium during equal channel angular pressing, Mater. Sci. Eng. A 527 (2010) 789–796.

[11] Y.J. Chen, Y.J. Li, X.J. Xu, J. Hjelen, H.J. Roven, Novel deformation structures of pure titanium induced by room temperature equal channel angular pressing, Mater. Lett. 117 (2014) 195–198.

[12] S.J. Lainé, K.M. Knowles, $\{11\bar{2}4\}$ deformation twinning in commercial purity titanium at room temperature, Philos. Mag. 95 (2015) 2153–2166.

[13] F. Xu, X.Y. Zhang, H.T. Ni, Q. Liu, $\{11\bar{2}4\}$ deformation twinning in pure Ti during dynamic plastic deformation, Mater. Sci. Eng. A 541 (2012) 190–195.

[14] J. Wang, S.K. Yadav, J.P. Hirth, C.N. Tomé, I.J. Beyerlein, Pure-Shuffle Nucleation of

Deformation Twins in Hexagonal-Close-Packed Metals, Mater. Res. Lett. 1 (2013) 126–132.

[15] S. Mendelson, Zonal dislocations and twin lamellae in h.c.p. metals, Mater. Sci. Eng. 4 (1969) 231–242.

[16] S. Vaidya, S. Mahajan, Accommodation and formation of $\{11\bar{2}1\}$ twins in Co single crystals, Acta Metall, 28 (1980) 1123–1131.

[17] Y. Minonishi, S. Ishioka, M. Koiwa, S. Morozumi, M. Yamaguchi, The core structures of a $\frac{1}{3}\langle\bar{1}\bar{1}23\rangle\{11\bar{2}2\}$ edge dislocation under applied shear stresses in an h.c.p. model crystal, Philos. Mag. A 45 (1982) 835–850.

[18] L. Capolungo, I.J. Beyerlein, Nucleation and stability of twins in hcp metals, Phys. Rev. B 78 (2008) 024117.

[19] R. Aghababaei, S.P. Joshi, Micromechanics of tensile twinning in magnesium gleaned from molecular dynamics simulations, Acta Mater. 69 (2014) 326–342.

[20] Y.T. Zhu, X.Y. Zhang, H.T. Ni, F. Xu, J. Tu, C. Lou, Formation of $\{11\bar{2}1\}$ twins in polycrystalline cobalt during dynamic plastic deformation, Mater. Sci. Eng. A 548 (2012) 1–5.

[21] E. Faran, D. Shilo, Twin Motion Faster Than the Speed of Sound, Phys. Rev. Lett. 104 (2010) 155501.

[22] N.J. Lane, S.I. Simak, A.S. Mikhaylushkin, I.A. Abrikosov, L. Hultman, M.W. Barsoum, First-principles study of dislocations in hcp metals through the investigation of the $(11\bar{2}1)$ twin boundary, Phys. Rev. B 84 (2011) 184101.

[23] E.J. Freise, A. Kelly, Twinning in Graphite, Proc. Royal Society A 264 (1961) 269–276.

[24] R.W. Cahn, Survey of recent progress in the field of deformation twinning, in: R.E. Reed-Hill, P. Hirth, H.C. Rogers, (eds.), Deformation Twinning, Gordon and Breach Science Publishers, New York, 1964, pp. 1–28.

[25] R. Bullough, Deformation Twinning in the Diamond Structure, Proc. Phys. Soc. A 24 (1957) 568–577.

[26] J.B. Hess, C.S. Barrett, Structure and nature of kink bands in zinc, Trans. AIME 185 (1949) 599–606.

[27] K. Hagihara, M. Yamasaki, M. Honnami, H. Izuno, M. Tane, T. Nakano, Y. Kawamura, Crystallographic nature of deformation bands shown in Zn and Mg-based long-period stacking ordered (LPSO) phase, Philos. Mag. 95 (2015) 132–157.

[28] F. Xu, X.Y. Zhang, H.T. Ni, Y.M. Cheng, Y.T. Zhu, Q. Liu, Effect of twinning on microstructure and texture evolutions of pure Ti during dynamic plastic deformation, Mater. Sci. Eng. A 564 (2013) 22–33.

[29] X.Y. Zhang, Y.T. Zhu, Q. Liu, Deformation twinning in polycrystalline Co during room temperature dynamic plastic deformation, Scr. Mater. 63 (2010) 387–390.

[30] Y.S. Li, N.R. Tao, K. Lu, Microstructural evolution and nanostructure formation in copper during dynamic plastic deformation at cryogenic temperatures, Acta Mater. 56 (2008) 230–241.

[31] Y. Zhang, N.R. Tao, K. Lu, Effects of stacking fault energy, strain rate and temperature on microstructure and strength of nanostructured Cu–Al alloys subjected to plastic deformation, Acta Mater. 59 (2011) 6048–6058.

[32] H.T. Wang, N.R. Tao, K. Lu, Strengthening an austenitic Fe–Mn steel using nanotwinned austenitic grains, Acta Mater. 60 (2012) 4027–4040.

[33] S.B. Jin, N.R. Tao, K. Marthinsen, Y.J. Li, Deformation of an Al–7Mg alloy with extensive structural micro-segregations during dynamic plastic deformation, Mater. Sci. Eng. A 628 (2015) 160–167.

[34] A. Akhtar, Basal slip and twinning in α-titanium single crystals, Metall. Mater. Trans. A 6 (1975) 1105–1113.

[35] F.D. Rosi, Mechanism of Plastic Flow in Titanium: Manifestations and Dynamics of Glide, Trans. AIME 200 (1954) 58–69.

[36] A.G. Crocker, J.S. Abell, The crystallography of deformation kinking, Philos. Mag. 33 (1976) 305–310.

[37] E. Orowan, A type of plastic deformation new in metals, Nature 149 (1942) 643–644.

[38] C.S. Lee, B.J. Duggan, R.E. Smallman, A theory of deformation banding in cold rolling, Acta Metal. Mater. 41 (1993) 2265–2270.

[39] D. Kuhlmann-Wilsdorf, “REGULAR” Deformation Bands (DBs) and the LEDS Hypothesis, Acta Mater. 47 (1999) 1697–1712.

[40] R. Matsumoto, M. Uranagase, N. Miyazaki, Molecular Dynamics Analyses of Deformation Behavior of Long-Period-Stacking-Ordered Structures, Mater. Trans. 54 (2013) 686–692.

[41] K. Hagihara, M. Honnami, R. Matsumoto, Y. Fukusumi, H. Izuno, M. Yamasaki, T. Okamoto, T. Nakano, Y. Kawamura, In-situ observation on the formation behavior of the deformation kink bands in Zn single crystal and LPSO phase, Mater. Trans. 56 (2015)

943–951.

[42] A.T. Churchman, The Slip Modes of Titanium and the Effect of Purity on their Occurrence during Tensile Deformation of Single Crystals, Proc. R. Soc. Lond. A 226 (1954) 216–226.

[43] A.A. Salem, S.R. Kalidindi, S.L. Semiatin, Strain hardening due to deformation twinning in α-titanium: Constitutive relations and crystal-plasticity modeling, Acta Mater. 53 (2005) 3495–3502.

[44] J.C. Gong, A.J. Wilkinson, Anisotropy in the plastic flow properties of single-crystal α titanium determined from micro-cantilever beams, Acta Mater. 57 (2009) 5693–5705.

[45] X.L. Nan, H.Y. Wang, L. Zhang, J.B. Li, Q.C. Jiang, Calculation of Schmid factors in magnesium: Analysis of deformation behaviors, Scr. Mater. 67 (2012) 443–446.

[46] X.L. Nan, H.Y. Wang, Z.Q. Wu, E.S. Xue, L. Zhang, Q.C. Jiang, Effect of c/a axial ratio on Schmid factors in hexagonal close-packed metals, Scr. Mater. 68 (2013) 530–533.

[47] A.T Churchman, The yield phenomena, kink bands and geometric softening in titanium crystals, Acta Metall. 3 (1955) 22–29.

[48] S.B. Jin, K. Zhang, R. Bjørge, N.R. Tao, K. Marthinsen, K. Lu, Y.J. Li, Formation of incoherent deformation twin boundaries in a coarse-grained Al-7Mg alloy, Appl. Phys. Lett. 107 (2015) 091901.

[49] T.G. Carnahan, Small angle tilt and twist grain boundary strengthening in yttrium, Retrospective Theses and Dissertations, Iowa State University, 1971.

Table. 1 Calculation results of SFs for basal- and prismatic-$\langle a \rangle$ slip systems in grains 1-6.

		Grain1	DB1	Grain2	DB2	Grain3	DB3
Basal slip systems	$(0001)[\bar{1}\bar{1}20]$	0.14	0.46	0.16	0.31	0.38	0.31
	$(0001)[\bar{1}2\bar{1}0]$	0.38	0.1	0.3	0.18	0.2	0.45
	$(0001)[2\bar{1}\bar{1}0]$	0.24	0.35	0.14	0.49	0.18	0.14
Prismatic slip systems	$(1\bar{1}00)[11\bar{2}0]$	0.27	0.1	0.4	0.2	0.03	0.15
	$(10\bar{1}0)[1\bar{2}10]$	0.13	0.07	0.03	0.14	0.37	0.06
	$(0\bar{1}10)[\bar{2}110]$	0.04	0.18	0.38	0.06	0.34	0.09

		Grain4	DB4	Grain5	DB5	Grain6	DB6
Basal slip systems	$(0001)[\bar{1}\bar{1}20]$	0.49	0.22	0.36	0.46	0.08	0.5
	$(0001)[\bar{1}2\bar{1}0]$	0.31	0.35	0.23	0.31	0.12	0.24
	$(0001)[2\bar{1}\bar{1}0]$	0.19	0.03	0.13	0.15	0.2	0.26
Prismatic slip systems	$(1\bar{1}00)[11\bar{2}0]$	0.07	0.09	0.14	0.13	0.35	0.01
	$(10\bar{1}0)[1\bar{2}10]$	0.23	0.07	0.41	0.23	0.46	0.24
	$(0\bar{1}10)[\bar{2}110]$	0.16	0.02	0.28	0.21	0.11	0.25

Figure captions:

Fig. 1. (a) Initial grain structure of DPD sample in the cross section normal to compression direction (CD); and (b) corresponding texture measured on the compression plane.

Fig. 2. (a) Twin boundaries formed in DPD sample with $\varepsilon = 0.29$; (b) misorientation distribution and inverse pole figures showing the misorientation axis for grain boundaries of selected twin boundary misorientation angles; (c) and (d) EBSD maps of grains 2 and 3 in (a), respectively; and (e) T2 twinning formed in the sample with $\varepsilon = 0.20$. Variation of misorientation peak values corresponding to T1, T2 and C1 twins in samples deformed to different deformation strains are also listed in the inserted table.

Fig. 3. (a) EBSD map for grain 1 in Fig. 2; (b) misorientation distribution along the grain boundary between DB1 and Grain 1 (the orientation was measured from left to right); (c) $\{10\bar{1}0\}$ and $\{11\bar{2}1\}$ pole figures for DB1 and grain matrix; and (d) inverse pole figure showing the misorientation axes for DB1 boundaries. The arrowed line in (a) is to show the common trace of $\{11\bar{2}1\}$ planes of DB1 and surrounding matrix crystal.

Fig. 4. (a) and (b) EBSD maps of kink bands formed in the DPD samples with $\varepsilon = 0.09$ and 0.20 respectively; (c) kernel orientation spread map of grains in (b); (d) and (e) $\{10\bar{1}0\}$ and $\{11\bar{2}1\}$ pole figures for grains 5 and 6, respectively; and (f) schematic drawing for rotation $\{11\bar{2}1\}$ planes in kink band/matrix crystal. The arrowed lines in (d) and (e) indicate the trace of $\{11\bar{2}1\}$ planes of surrounding matrix crystals close to the kind band boundary traces.

Fig. 5. (a) and (b) Schmid factors (SFs) for basal- and prismatic-⟨a⟩ dislocation slip systems in

six kink bands and corresponding six grain matrix crystals in the DPD samples (grains 1-6), respectively; and (c) stereographic projection of the loading directions in grains 1-6.

Fig. 6. (a) Schematic drawing on the relation of loading direction with $[10\bar{1}0]$ axis (OM: loading direction; OM′: projection of OM on $(10\bar{1}0)$ plane; θ: angle between loading direction and $[10\bar{1}0]$ axis, ω: angle between OM′ and c axis); and (b-f) SF values of basal-$\langle a \rangle$, prismatic-$\langle a \rangle$, and T2 twin variants as a function of ω at θ = 50.8º, 63.4, 70º, 85.2º and 90º, respectively. The dashed segments of SF curves of T2 twin variants denote the SFs with negative sign. The basal and basal dislocation slip variants are represent by B1~B3, and P1~P3, respectively. The variants of T2 twin are represented by T21~T26.

Fig. 7. (a)-(c) Schematic of formation and evolution of a DB in a grain with initial orientation θ=90° and ω=37.5°; (d) SF variation of the DB and the matrix with lattice rotation; and (e) $(10\bar{1}0)$ plane view of the T2 twin boundaries. Pink and gray atoms correspond to the alternate stacks.

Fig. 8. Length fraction of T2 twin boundaries in grain boundaries with misorientation angles larger than 5º (%), and the absolute length of T2 twin boundaries per unit area in the DPD samples subjected to different deformation strain.

Fig. 9. (a) and (b) T2 twin boundaries connecting to high angle kink boundaries formed in the DPD samples with ε = 0.71 and 1.13, respectively; (c) and (d) inverse pole figures showing the misorientation axis of twin/kink band boundaries to (a) and (b) respectively. The poles encircled by dotted lines of different colors are corresponding to the boundary segments encircled by

dotted lines of same colors in (a) and (b).

Fig. 10. (a) and (b) deviation of the misorientation angle of T1 and C1 TBs formed in the DPD sample with $\varepsilon = 0.29$; (c) and (d) corresponding inverse pole figures showing the misorientation axis of twin boundaries of grains in (a) and (b), respectively. The points encircled by the black dotted lines are corresponding to the misorientation axes for the black boundary segments surrounding the twin crystals.

Figure(s)

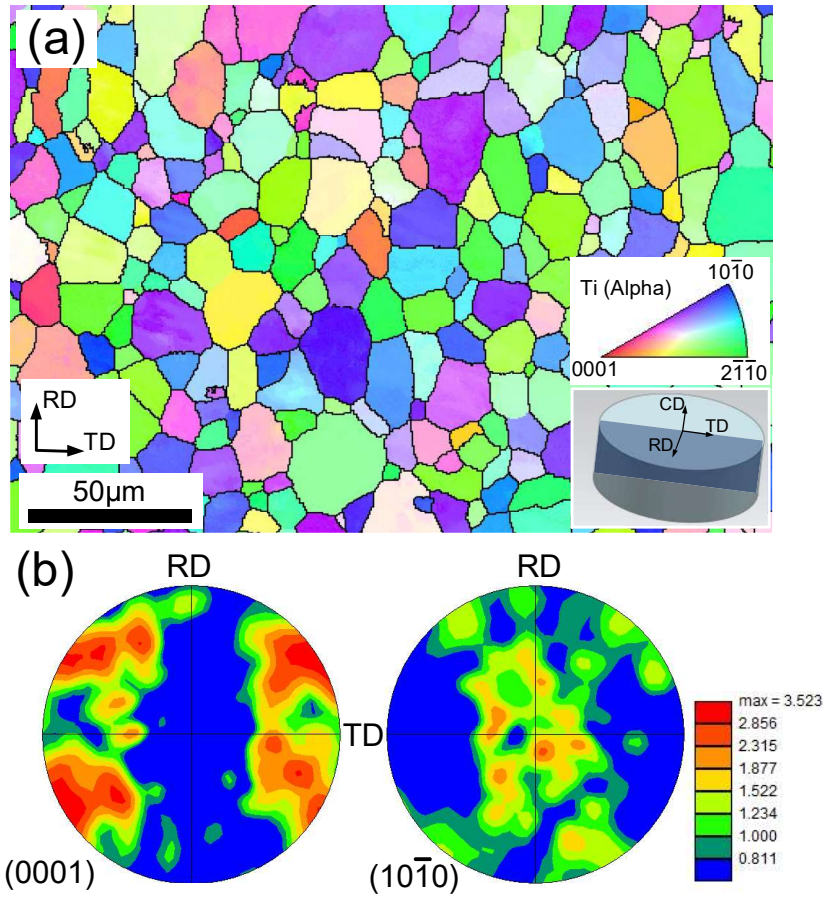

Fig. 1. (a) Initial grain structure of DPD sample in the cross section normal to compression direction (CD); and (b) corresponding texture measured on the compression plane.

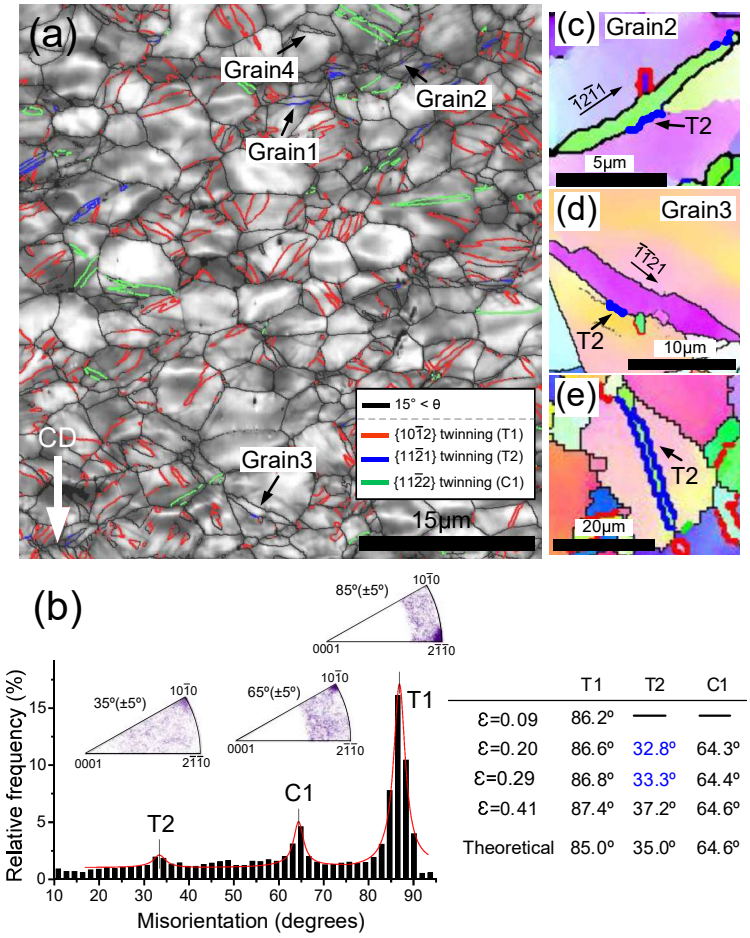

	T1	T2	C1
ε=0.09	86.2°	—	—
ε=0.20	86.6°	32.8°	64.3°
ε=0.29	86.8°	33.3°	64.4°
ε=0.41	87.4°	37.2°	64.6°
Theoretical	85.0°	35.0°	64.6°

Fig. 2. (a) Twin boundaries formed in DPD sample with ε = 0.29; (b) misorientation distribution and inverse pole figures showing the misorientation axis for grain boundaries of selected twin boundary misorientation angles; (c) and (d) EBSD maps of grains 2 and 3 in (a), respectively; and (e) T2 twinning formed in the sample with ε = 0.20. Variation of misorientation peak values corresponding to T1, T2 and C1 twins in samples deformed to different deformation strains are also listed in the inserted table.

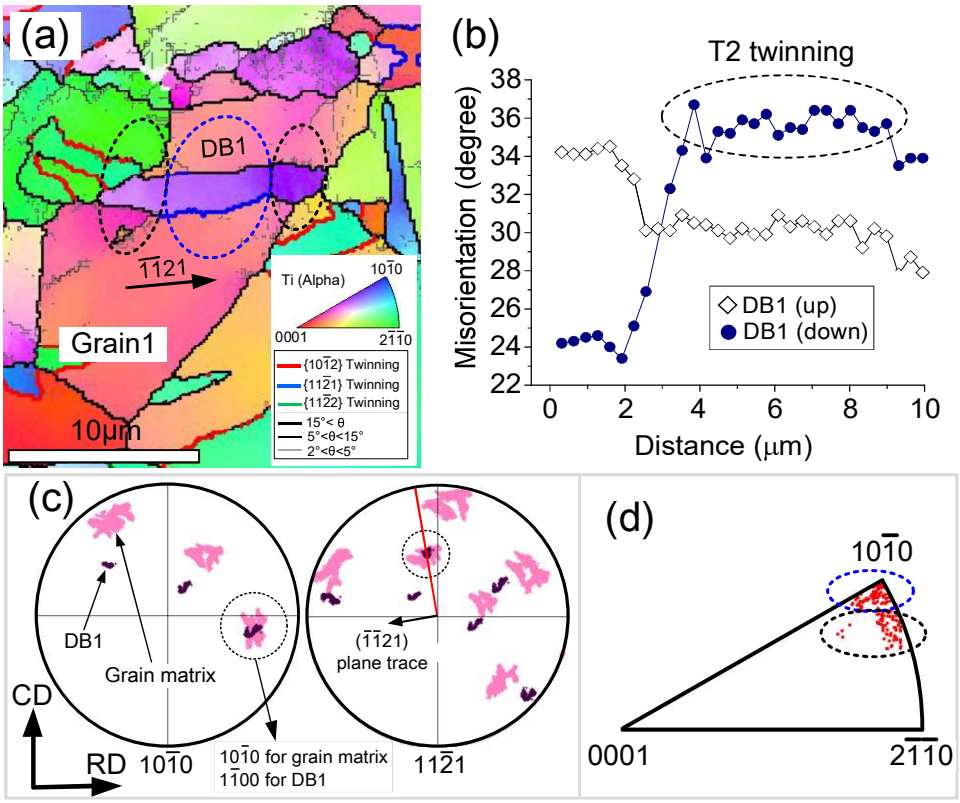

Fig. 3. (a) EBSD map for grain 1 in Fig. 2; (b) misorientation distribution along the grain boundary between DB1 and Grain 1 (the orientation was measured from left to right); (c) $\{10\bar{1}0\}$ and $\{11\bar{2}1\}$ pole figures for DB1 and grain matrix; and (d) inverse pole figure showing the misorientation axes for DB1 boundaries. The arrowed line in (a) is to show the common trace of $\{11\bar{2}1\}$ planes of DB1 and surrounding matrix crystal.

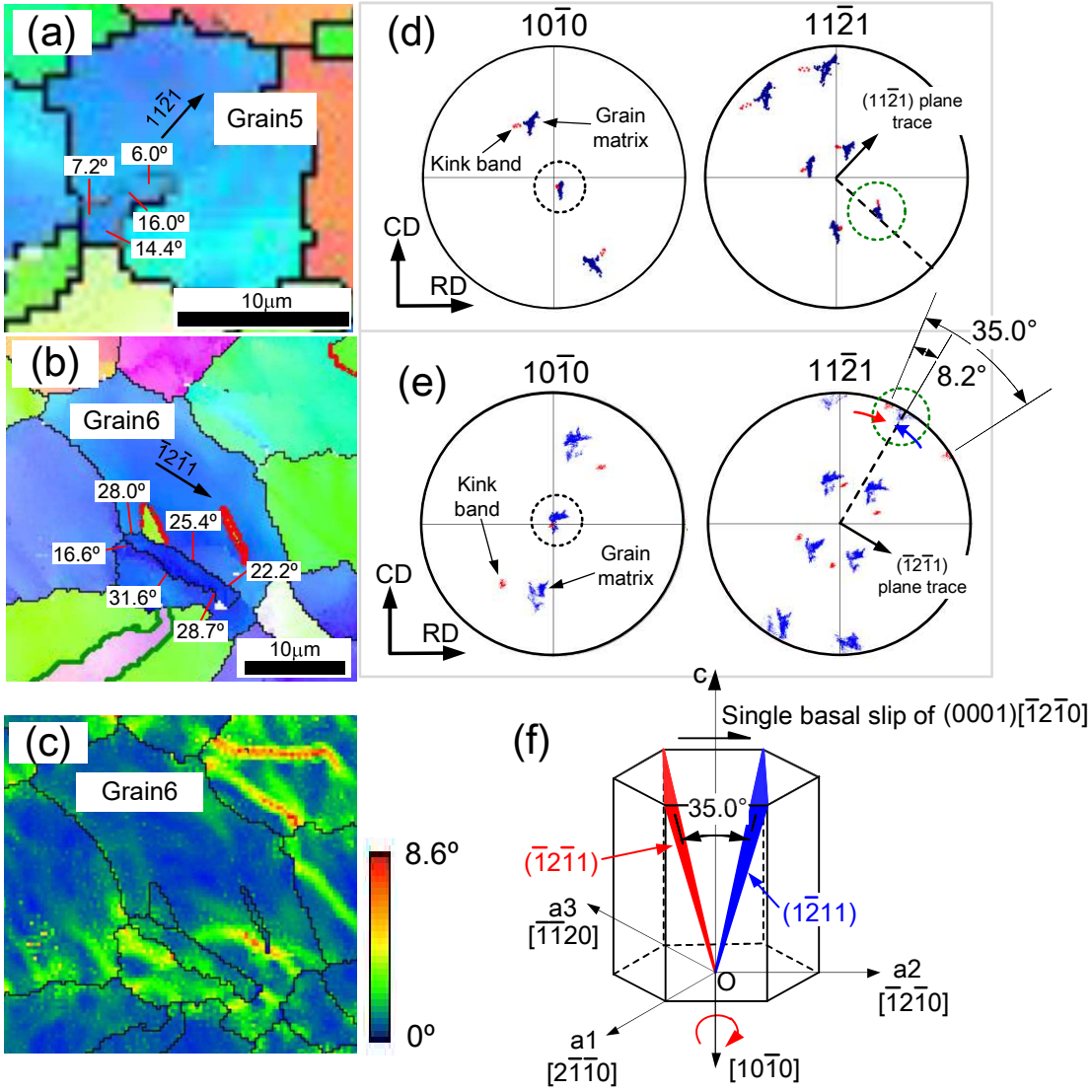

Fig. 4. (a) and (b) EBSD maps of kink bands formed in the DPD samples with ε = 0.09 and 0.20 respectively; (c) kernel orientation spread map of grains in (b); (d) and (e) $\{10\bar{1}0\}$ and $\{11\bar{2}1\}$ pole figures for grains 5 and 6, respectively; and (f) schematic drawing for rotation $\{11\bar{2}1\}$ planes in kink band/matrix crystal. The arrowed lines in (d) and (e) indicate the trace of $\{11\bar{2}1\}$ planes of surrounding matrix crystals close to the kind band boundary traces.

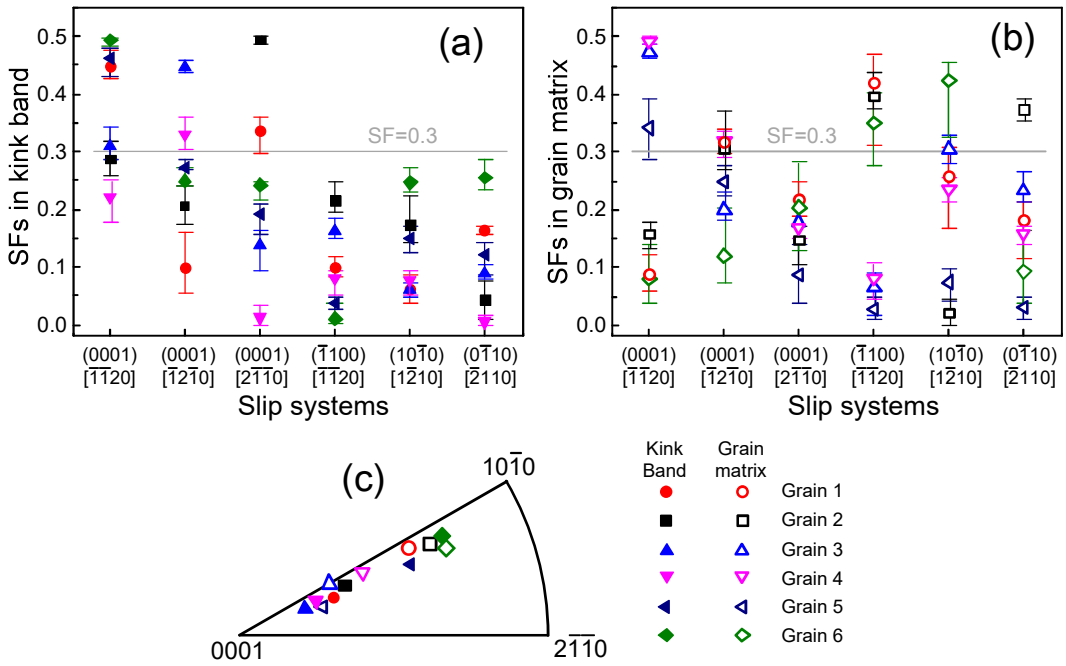

Fig. 5. (a) and (b) Schmid factors (SFs) for basal- and prismatic-⟨a⟩ dislocation slip systems in six kink bands and corresponding six grain matrix crystals in the DPD samples (grains 1-6), respectively; and (c) stereographic projection of the loading directions in grains 1-6.

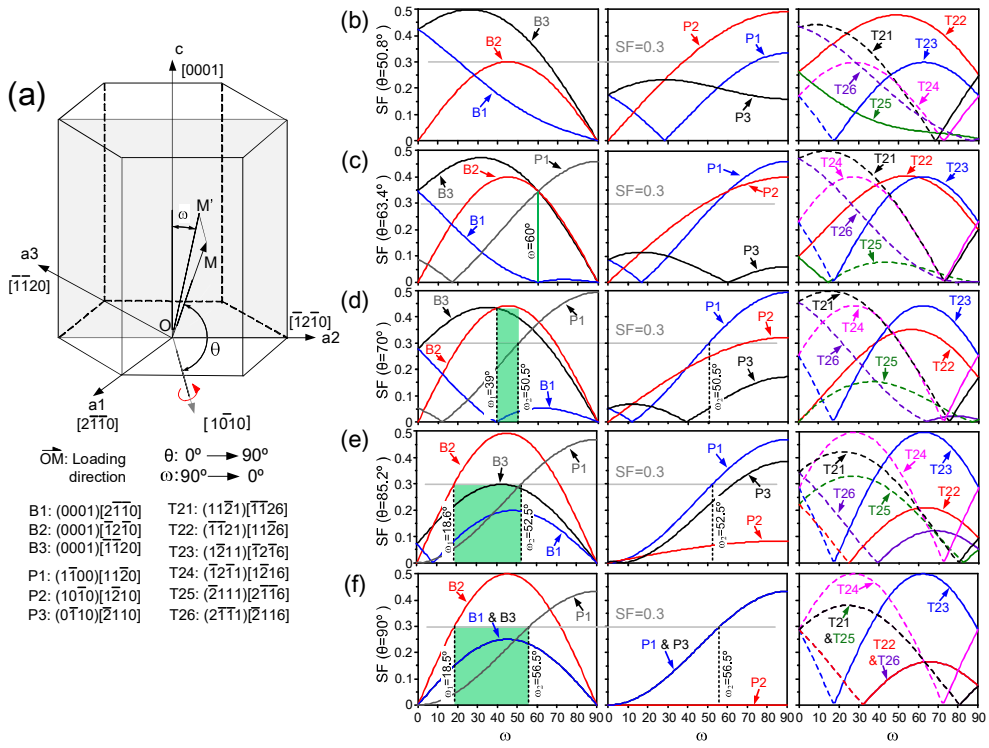

Fig. 6. (a) Schematic drawing on the relation of loading direction with $[10\bar{1}0]$ axis (OM: loading direction; OM′: projection of OM on $(10\bar{1}0)$ plane; θ: angle between loading direction and $[10\bar{1}0]$ axis, ω: angle between OM′ and c axis); and (b-f) SF values of basal-$\langle a \rangle$, prismatic-$\langle a \rangle$, and T2 twin variants as a function of ω at θ = 50.8º, 63.4, 70º, 85.2º and 90º, respectively. The dashed segments of SF curves of T2 twin variants denote the SFs with negative sign. The basal and basal dislocation slip variants are represent by B1~B3, and P1~P3, respectively. The variants of T2 twin are represented by T21~T26.

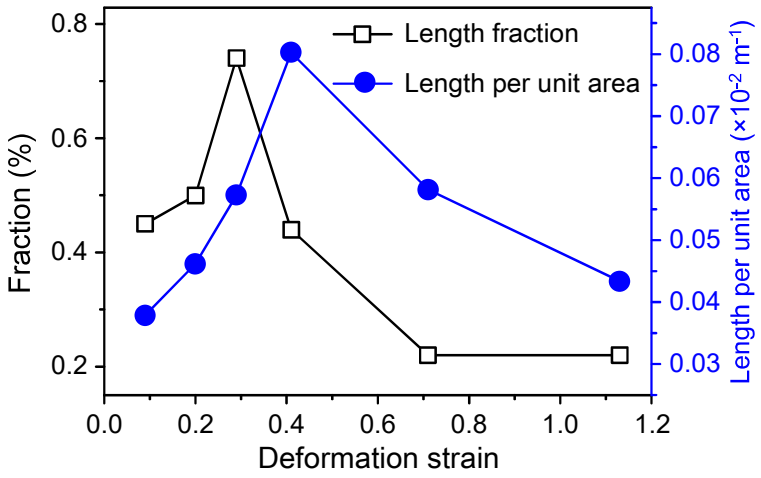

Fig. 7. Length fraction of T2 twin boundaries in grain boundaries with misorientation angles larger than 5º (%), and the absolute length of T2 twin boundaries per unit area in the DPD samples subjected to different deformation strain.

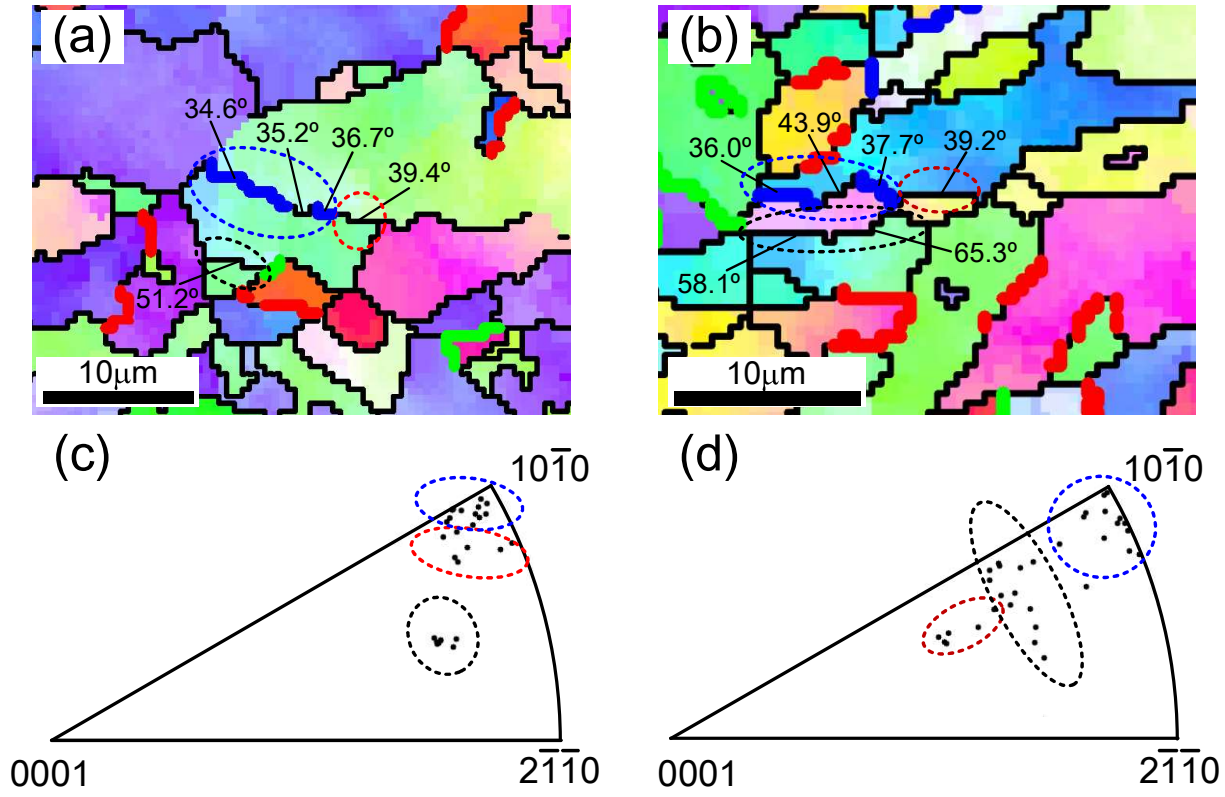

Fig. 8. (a) and (b) T2 twin boundaries connecting to high angle kink boundaries formed in the DPD samples with ε = 0.71 and 1.13, respectively; (c) and (d) inverse pole figures showing the misorientation axis of twin/kink band boundaries to (a) and (b) respectively. The poles encircled

by dotted lines of different colors are corresponding to the boundary segments encircled by dotted lines of same colors in (a) and (b).

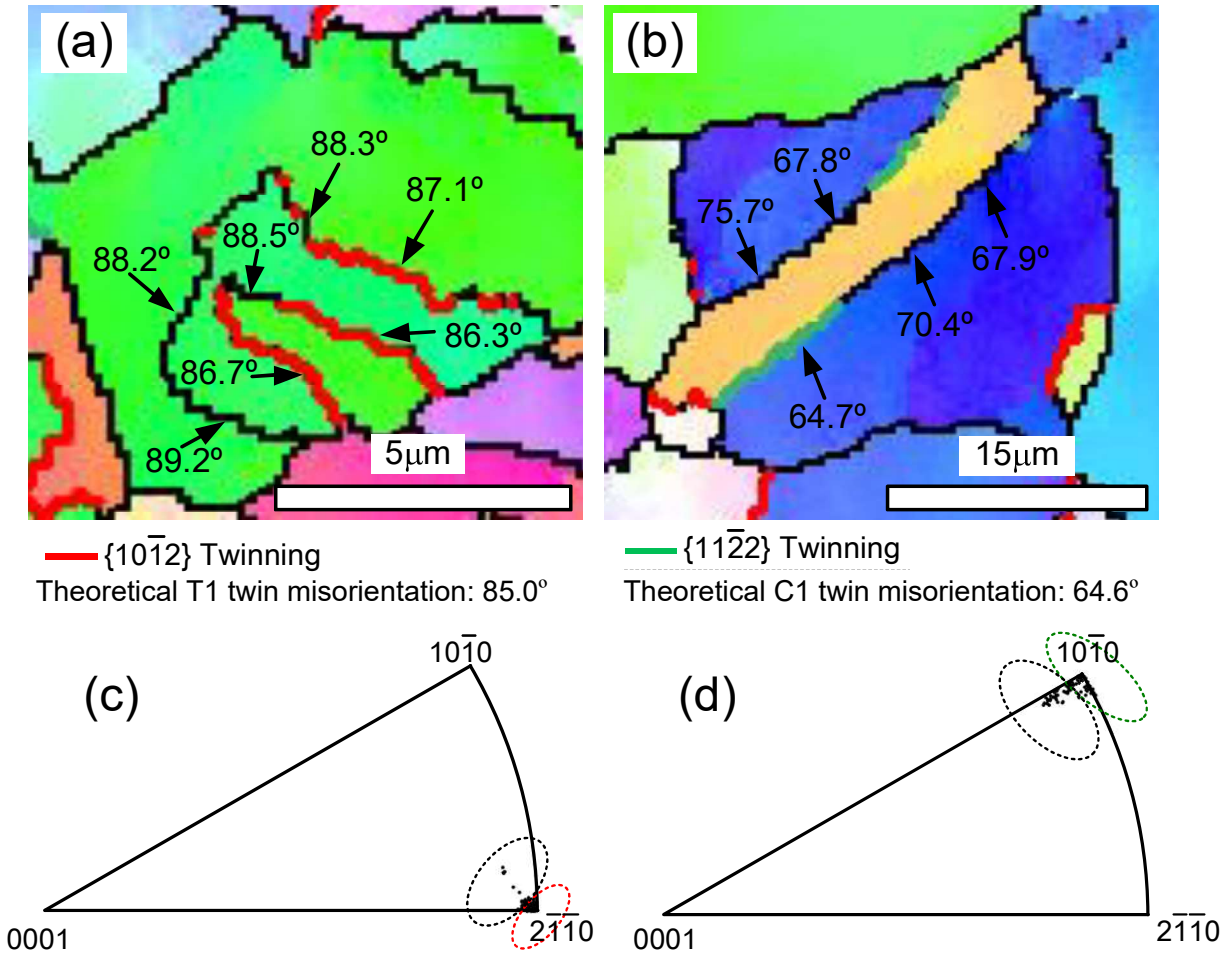

Fig. 9. (a) and (b) deviation of the misorientation angle of T1 and C1 TBs formed in the DPD sample with ε = 0.29; (c) and (d) corresponding inverse pole figures showing the misorientation axis of twin boundaries of grains in (a) and (b), respectively. The points encircled by the black dotted lines are corresponding to the the misorientation axes for the black boundary segments surrounding the twin crystals.

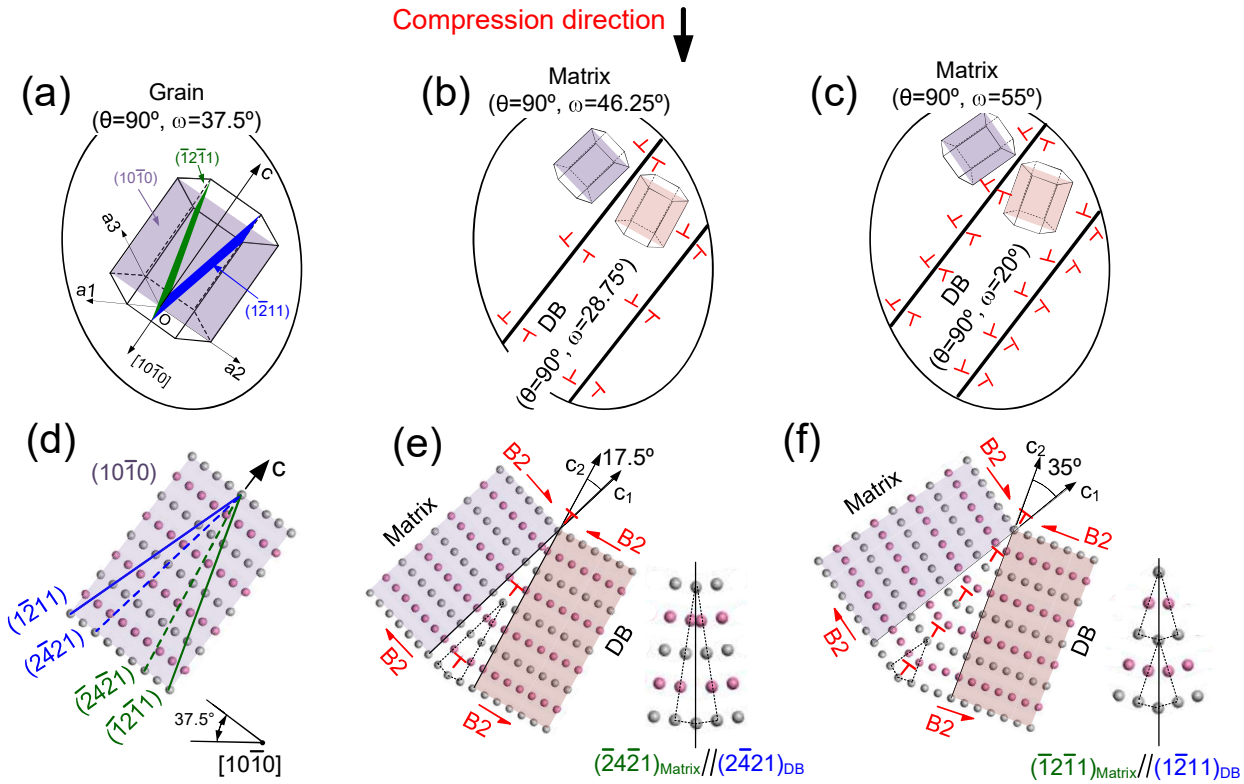

Fig. 10. (a)-(c) Schematic of formation and evolution of a DB in a grain with initial orientation θ=90° and ω=37.5°; and (d)-(f) $(10\bar{1}0)$ plane view of the initial matrix, low angle DBs and T2 twin boundaries, respectively. Pink and gray atoms correspond to the alternate stacks.

*Graphical Abstract